Estimating latent heat over a melting arctic snow cover

Annette Semadeni-Davies[1,2], David Maréchal[3,4], Oddbjørn Bruland[2,3], Yuji Kodama[5] and Knut Sand[3,6]

[1]Department of Water Resources Engineering, Lund University, Box 118, SE-22100 Lund, Sweden
Tel: +46 46 222 4165; fax: +46 46 222 4435; E-mail: *annette.davies@tvrl.lth.se*
[2]Department of Hydraulic and Environmental Engineering, Norwegian University of Science and Technology, Trondheim, Norway
[3]SINTEF Civil and Environmental Engineering, Trondheim, Norway
[4]Institute of Water and Environment, Cranfield University at Silsoe, Bedfordshire, UK
[5]Institute of Low Temperature Science, Hokkaido University, Sapporo 060-0819, Japan
[6]Statkraft Grøner AS, Trondheim, Norway

Received 15 November 2002; accepted in revised form 11 December 2003

Abstract The latent heat flux over snow near Ny-Ålesund, Spitsbergen, was investigated for the 1999 snowmelt season to assess different methods of modelling the flux. Snow evaporation had hitherto been estimated as the residual of plot water balance calculations and was subject to measurement errors: hence a modelling solution was sought to make use of existing data. Precipitation, snow depth and albedo were measured daily. Runoff from the plots was recorded continuously. Wind speed, relative humidity and air temperature were measured at two levels (2 and 10 m) every 10 minutes; wind direction was noted hourly. Three models which simulate latent heat were assessed against evaporation and condensation measured by weighing several snow-filled containers each day. Two employ the bulk profile method (within the SNTHERM and CROCUS snowmelt models), while the third is the aerodynamic profile method (APM). Each follows the measured evaporation until snow-free patches develop after which the APM predicts evaporation whereas the snowmelt models predict condensation. The effect of wind is also noted. A major conclusion of this work is that the complexity of the land surface/atmosphere interactions, particularly when the snow cover breaks up, precludes the use of simple models for determining latent heat.

Keywords Aerodynamic profile method; bulk profile method; CROCUS; snow-free patches; SNTHERM; wind direction

Nomenclature and abbreviations

APM	aerodynamic profile method
BPM	bulk profile method
SINTEF	Foundation for Scientific and Industrial Research at the Norwegian Institute of Technology
IHL	Institute of Hydrology lower runoff plot
IHU	Institute of Hydrology upper runoff plot
LAPP	Land Arctic Physical Processes
DNMI	Norwegian Meteorological Institute
LH Sør	SINTEF Leirhaugen South runoff plot
SWE	snow water equivalent
g ($\mathrm{m\,s^{-2}}$)	acceleration due to gravity
ρ ($\mathrm{kg\,m^{-3}}$)	air density
P_a (m bars)	air pressure
T (K)	air temperature
C_e	bulk transfer coefficient for water vapour
ϕ_m	dimensionless stability function for momentum

Nordic Hydrology **Vol 35 No 3 pp 175–190** © IWA Publishing 2004

ϕ_e	dimensionless stability function for vapour
u (m s^{-1})	horizontal wind speed
QE (W m^{-2})	latent heat flux
Lv (J kg^{-1})	latent heat of vapourisation
Ke (m^2 s^{-1})	latent heat turbulent transfer coefficient
z (m)	reference measurement height
Rh (%)	relative humidity
Ri	Richardson number
q_a (g g^{-1})	specific humidity (air) at observation level z
q_s (g g^{-1})	specific humidity at the snow surface
q (g g^{-1})	specific humidity
e_a (mbar)	vapour pressure of air
e_s (mbar)	vapour pressure, saturated over water
k	von Karmen's constant

Introduction

"The best-laid schemes o' mice an' men
Gang aft agley" Burns (1785)

This paper compares three methods to simulate latent heat in order to determine their suitability for application to a melting Arctic snow cover at Leirhaugen near Ny-Ålesund (78°55′N, 11°56′E), Spitsbergen Archipelago. It had originally been intended that evaporation from the snow cover be estimated as the residual term of the water balances of three runoff plots. However, various unforeseen problems, such as the formation of a thick basal ice layer above the soil surface, meant that this approach was subject to error. It was then decided that a modelling solution be found to make use of existing climate and snow data sets – the question was: which method best fitted the few direct observations of evaporation that were available? The simple answer is that none of the models was up to the task as melt progressed due to the heterogeneous, patchy nature of the snow cover and the fact that the input data were not collected for this purpose. Nonetheless, the study gives an insight into the real-world problems of snow modelling as well as identifying the factors most likely to lead to evaporation at the site.

Extensive snow, climate and runoff data has been collected at Leirhaugen by Norwegian (SINTEF, Foundation for Scientific and Industrial Research at the Norwegian Institute of Technology) and British (Centre for Ecology & Hydrology, formerly the Institute of Hydrology) researchers as part of the EU funded LAPP project (Land Arctic Physical Processes – contract no ENV4-CT95-0093). This project ran from 1996 to 1999 and was set up to investigate polar land/surface interactions with respect to climate change. Arctic regions are vulnerable to global warming, particularly regarding the timing of snow accumulation and melt. The length of the snow season largely controls the seasonal energy balance and determines the time available for soil active layer development and plant growth (Lloyd *et al.* 2001). Harding and Lloyd (1998) noted that year-to-year variability in the annual energy balance was related to the spring snow depth. This paper follows Bruland and Maréchal (1999), Bruland *et al.* (2001a) and Maréchal *et al.* (2002) who investigated the energy and water balances for the site during spring melt as part of the Norwegian contribution to LAPP. They note that knowing the latent heat flux is essential for both determining energy available for snowmelt and making water balance calculations, particularly soil water recharge in the active layer.

While eddy correlation observations are available for the 1995 and 1996 snow seasons (LAPP 1999; Harding and Lloyd 1998; Lloyd *et al.* 2001), the instruments were sent to other

sites within the project in order to keep costs down. Evaporation (and condensation) for the remaining snow seasons was to be estimated as the residual of the water balance on the basis of three runoff plots. It was assumed that there is no infiltration until the soil has thawed. However, flow through frozen soil and over thick layers of basal ice from outside the plots has been observed and freezing in the runoff gutters has caused blockages, resulting in delayed flow and water loss at the collection point (Bruland and Maréchal 1999; LAPP 1999). Clearly, a method to determine the latent heat exchanges over snow during and just prior to snowmelt would be valuable. However, the belated nature of this realisation meant that the method must make use of existing data. Thus the main objective of this paper is to compare methods of calculating latent heat in order to find the model best suited to the Leirhaugen environment and data. A secondary objective is to identify the land and atmospheric conditions that lead to a high latent heat flux.

Here, three methods to estimate the latent heat flux were compared for the 1999 snowmelt season against each other as well as against changes in water mass (i.e. evaporation/condensation) observed by weighing snow-filled plastic containers. The outputs were also compared to runoff plot data. The models are the bulk profile method (BPM), embedded in the SNTHERM and CROCUS snowpack models, and the aerodynamic profile method (APM). The two snow models were chosen as they are widely applied and represent the most sophisticated snow modelling packages currently available. The APM was included as it does not rely on snowpack simulation. The footprint of the APM data is large in comparison to the BPM input data due to the height of the top level of the meteorological tower (10 m) compared to the lower level (2 m). Thus, a true comparison between the methods is not strictly possible. Instead, readers should be aware that this paper offers a real-world study complete with all the problems inherent in using non-purposely collected data. The latent heat flux simulated using the APM is then related to surface and meteorological conditions in order to identify the factors most likely to lead to a high latent heat flux. It was found that the complexity of the land surface/atmosphere interactions makes modelling the latent heat flux dubious during late snowmelt when patches of bare soil are exposed.

Background

The turbulent fluxes of latent and sensible heat are driven by the vertical gradients of wind velocity, ambient air temperature and humidity. Latent heat over snow is generally negative, indicating sublimation (ice to vapour) or evaporation (water to vapour), due to the dryness of cold air compared to the snow surface (Male and Granger 1981). Whether a negative latent heat flux leads to sublimation or evaporation depends on the surface condition of the snow and the weather conditions: in either case, the energy is lost to snowmelt. Where there is advection of warm, moist air masses (e.g. Moore and Owen 1984) latent heat can be positive, leading to condensation on the snow surface and energy available for snowmelt. The latent heat of vaporisation ($2.53 \times 10^6\,\mathrm{W\,m^{-2}}$ at 0°C) is almost 7.5 times greater than that of fusion. Thus, even when the heat flux is large, the volume of water lost or added to the snowpack is likely to be low (e.g. Bengtsson 1980).

Previous studies of high-Arctic conditions show that the latent heat flux is variable. Liston and Sturm (2003) provide a comprehensive review of sublimation in the Arctic and conclude that sublimation can be a significant part of the winter moisture budget depending on weather conditions, particularly wind. Woo and Young (1997) investigated the Fosheim Peninsula, a polar oasis, in the Canadian Arctic; sublimation represented around 10–16% of the snow water equivalent (SWE) and the rate was sometimes in excess of $5\,\mathrm{mm\,d^{-1}}$. They cite other studies which show both greater (over 25%; Rydén 1977) and similar (Ohmura 1982) sublimation rates. On the basis of runoff plot data for five snow seasons, Kane *et al.* (1991) postulated that warm dry southerly air flowing over the Brooks Range to the northern coastal

plains of Alaska is likely to enhance latent heat exchanges. They estimate that around 20–30% of the SWE evaporated at the catchment scale. As part of the LAPP project, eddy correlation measurements for the 1995 and 1996 snow seasons (LAPP 1999; Harding and Lloyd 1998) gave seasonal values of 1 MJ m^{-2} and 6.7 MJ m^{-2}, respectively. Latent heat accounted for around 20–30% of the net all-wave radiation for both years but evaporation was less than 5% of the snow cover. This finding is similar to the modelled results presented below for the same site in 1999.

Methodology

Study site

Leirhaugen is a rise above a coastal plain and lies about 3 km west of Ny-Ålesund on the Brøggerhalvøya Peninsula on the west coast of Spitsbergen Island, Svalbard Archipelago. The site is on the floodplain of the Bayelva River. According to the Köppen system of climate classification, the area has a Polar Tundra climate (Hanssen-Bauer *et al.* 1990). Although also influenced by the cold East Greenland current, the climate is mild due to the warm Norwegian current that flows both north into the Barents Sea and along the western side of the archipelago. The annual mean temperature is -6.3°C and precipitation is 385 mm yr^{-1}. Snow begins to accumulate in September and melts in early June. Midnight sun occurs between 18 April and 24 August. Atmospheric circulation is influenced by the Icelandic Low and the high pressure over Greenland and the Arctic Ocean. Thus atmospheric conditions are strongly linked to wind direction. Westerly and south-westerly winds originate between Iceland and Norway, such winds bringing warm air masses from lower latitudes, while winds from the north and east are markedly colder.

To the west of Leirhaugen lies Mt Schetelig from which ridges extend from the west to the north-west. Beyond these ridges is open ocean. The north to east is bounded by the waters of Kongsfjord (King's Bay). From the east to south-east lie coastal hills and glaciers. High mountains and a glacial field lie to the south-east and south-west with the glacial terminal moraines between the south and west.

There are three runoff plots at the site maintained by SINTEF, two established by the Institute of Hydrology (Upper and Lower, IHU and IHL) and one by SINTEF (Leirhaugen South - LH Sør). Each has a different slope and aspect. In this paper the lower runoff plot (IHL) data are used as the plot is closest to the SINTEF meteorological tower. It is situated on the lower part of a gentle north-facing slope and has a surface area of 89.2 m^2 (Figure 1). The clayey upper soil is underlain by permafrost 100–400 m thick (Liestøl 1977), and the vegetation is low tundra scrub. The active layer varies between 80 and 100 cm. Snow and basal ice depths are measured daily at 14 points using stakes set in the clay around the plot perimeter. In order to preserve the snow surface, a nearby snow pit is used to determine both snow density and the vertical snow temperature profile. Observations at the snow pit are made daily. Plot runoff drains via a gutter directed into a tipping bucket rain gauge and the data logger (logging interval 10 min) is a Campbell CR10. Albedo measurements are carried out at the snow sampling points with a Kipp and Zonen Pyranometer CM.

There is a possibility that SWE, calculated as the product of depth and density observations, could contain errors as snow density was measured some metres from the plot. SWE compared favourably against precipitation at Ny-Ålesund (recorded daily by the Norwegian Meteorological Institute, DNMI). However, there may be differences in precipitation at the site and gauge 3 km distant.

Daily evaporation and condensation were measured for a short period (25 May–8 June) using two sets of three snow-filled plastic containers (10 cm depth, 18 cm × 18 cm width) – one near IHL and the other near LH Sør. These were weighed with the same spring scale (0–1000 g) to determine gains and losses in SWE. Edge effects and the albedo and thermal

Figure 1 IH lower runoff plot after melt showing snow depth measurement positions, walls and drainage gutter, 25 June 1999

properties of the containers are potential sources of error. The containers were installed in carefully excavated pits, so that the edge of each was at the same level as the surrounding snow surface. However, it was not possible to restore a natural snow surface, and surface albedo and surface roughness may be different from the natural snow surface. As snowmelt progressed the snow surface settled, leaving the walls of the container exposed above the snow surface, which introduced an aerodynamic barrier. For this reason the containers were topped-up after each weighing and replaced flush with the snowpack. There is also a possibility that the penetration of solar radiation through the snow could have heated the container, causing melt and the formation of a saturated layer at the container base; however, this was not observed.

The meteorological tower, installed in autumn 1998, is instrumented with Aanderaa sensors set at 2 and 10 m above the ground. The tower is around 40 m from the IHL runoff plot. Table 1 gives the manufacturer's estimates of accuracy: the instruments were also calibrated by the manufacturer (http://www.aanderaa.no/PDF_Files/RelHumd3445D271.pdf, date last checked 27 November 2003). Air temperature, wind speed, air humidity and incoming and outgoing short-and net all-wave radiation are recorded every 10 min with a Aanderaa Sensor Scanning Unit and an Aanderaa Data Storing Unit. The tower was consistently above snow rather than bare soil during melt. Wind direction is recorded hourly

Table 1 Sensor descriptions for the meteorological tower. Accuracy comes from the manufacturer (Aanderaa sensors)

Sensor	Unit	Accuracy
Wind speed	$m\,s^{-1}$	$\pm 2\%$ or $\pm 20\,cm\,s^{-1}$
Relative humidity	%	$\pm 3\%$
Temperature	°C	$\pm 0.1\%$ of range
Net radiation (incoming)	$W\,m^{-2}$	$\pm 1\%$ of full range
Net radiation (outgoing)	$W\,m^{-2}$	$\pm 1\%$ of full range
Solar radiation (incoming)	$W\,m^{-2}$	Better than $\pm 20\,W\,m^{-2}$
Solar radiation (outgoing)	$W\,m^{-2}$	Better than $\pm 20\,W\,m^{-2}$

at Ny-Ålesund by DNMI. A fuller description of the field campaign is given in Bruland and Maréchal (1999), Maréchal *et al.* (2002) and Bruland *et al.* (2001a).

Models

The turbulent fluxes of sensible and latent heat occur simultaneously and can be considered as a single process (Kuusisto 1986). The two fluxes are calculated by similar methods. However, only the latent heat flux is discussed further here. The effect of blowing snow on snow distribution and sublimation was not considered as the snowpack was isothermal and wet for the entire investigation period following a brief melt episode in early May. Three sets of formulae for determining the latent heat flux are used here; two are bulk or mean profile methods (embedded within full snowpack energy balance models), which require meteorological observations from one height above the snowpack, while the third is an aerodynamic profile method that utilises meteorological observations from the two levels of the instrument tower.

The ripe snow conditions lead to the assumption within the APM method that evaporation was more likely than sublimation. Assuming that the latent heat flux, Q_E, can be characterised by the vertical gradient of the mean specific humidity, the flux can be written as

$$Q_E = \rho_a L_v K_e \delta q / \delta z \tag{1}$$

where ρ is the air density, L_v is the latent heat of vaporisation, K_e is the latent heat turbulent transfer coefficient and z is the reference height of the humidity measurements. Specific humidity, q, represents the ratio of grams of vapour to grams of air and is related to vapour pressure, e_a, and air pressure, P_a, by (Saucier 1983)

$$q = 0.622(e_a)/P_a - 0.378(e_a). \tag{2}$$

In turn, vapour pressure, e_a, is determined from the relative humidity, Rh, and air temperature, T, following the Magnus–Tetens equation for saturated vapour pressure over water, e_s:

$$\begin{aligned} e_s &= 0.1 \times 10^{7.5T/(T+237.3)+2.7858} \\ e_a &= e_s Rh/100 \end{aligned} \tag{3}$$

The transfer coefficient can be calculated as a function of the wind profile given the similarity in the transfer of momentum, vapour and heat (see Anderson 1976). Thus, assuming a logarithmic profile, Eq. (1) can be expanded to

$$Q_E = \rho_a L_v k^2 [(u_2 - u_1)(q_2 - q_1)/\ln^2(z_2/z_1)][\phi_m \phi_e]^{-1} \tag{4}$$

where k is von Karmen's constant, u is the horizontal wind speed and ϕ_m and ϕ_e are dimensionless stability functions for momentum and vapour, respectively. Equation (4) is the basis of the APM method. The stability functions, at a point midway between z_1 and z_2, can be determined from the critical Richardson number:

$$Ri = 2g[(z_2 - z_1)(T_2 - T_1)]/[(T + T_1)(u_2 - u_1)^2] \tag{5}$$

where g is the acceleration due to gravity. For neutral conditions (i.e. the atmospheric temperature profile is adiabatic with no buoyancy effects) ϕ_m/ϕ_e is equal to unity. A positive Richardson number indicates a stable atmosphere (warm air over a cold surface) and a negative number unstable conditions. Businger (1973) suggests that, when the Richardson number is greater than values in the range of $+0.15$–0.25, atmospheric flow is virtually laminar with little vertical mixing. Here, $+0.19$ is set as a maximum value and the relationship between the two stability functions and the Richardson number is (Ohmura 1981; Cline 1997)

$$\phi_m = (1 - 18Ri)^{-0.25} \quad Ri < 0$$
$$\phi_m = (1 - 5.2Ri)^{-1} \quad Ri \geq 0 \tag{6}$$

for the momentum stability factor and

$$\phi_e = 1.3\phi_m \quad Ri < -0.03$$
$$\phi_e = \phi_m \quad Ri \geq -0.03 \tag{7}$$

for the vapour stability factor.

The APM has the disadvantage that it requires at least two sets of meteorological data. For this reason many snow modellers use the bulk profile method which has the basic form

$$Q_E = \rho_a L_v C_e (q_a - q_s) \tag{8}$$

where C_e is the bulk transfer coefficient for water vapour (Deardoff 1968) and q_a and q_s are the specific humidity at observation level z_a and at the snow surface, respectively. The bulk profile method is dependent on snow surface temperature and humidity, which in turn depend on the snowpack energy and mass fluxes.

The BPM equations used here are embedded within two physically based snowmelt models: CROCUS (Brun *et al.* 1989, 1992) and SNTHERM (Jordan 1991). Both are one-dimensional and have similar levels of complexity. They were run with hourly meteorological data from the 2 m level of the tower and were initialised according to the observed snow properties at the IHL plot and the snow pit.

Simulated snow surface energy exchanges with the atmosphere are short- and long-wave radiation, with sensible and latent heat and heat advection from precipitation. The models differ in their treatment of the bulk transfer coefficient for both the latent and sensible heat fluxes. CROCUS has a default setting where C_e was empirically determined for the Météo France, Col de Porte alpine research station: no changes for the Arctic location were made here. The latent heat flux in SNTHERM is calculated according to Andreas and Murphy (1986). The bulk transfer coefficient is determined in terms of the drag coefficient (this represents the bulk transfer of momentum under neutral conditions), snow roughness length and the measurement reference heights for wind speed and relative humidity. The stability factors for the transfer of momentum and water vapour, ϕ_m and ϕ_e, used in the calculation of C_e are found according to Anderson (1976).

Brun *et al.* (1992) tested the turbulent fluxes within CROCUS against hourly snow surface temperature. They found a very high ($R^2 = 0.97$) correlation for 2400 data points at Col de Porte. Essery *et al.* (1999) made a similar comparison of CROCUS against other snowpack models and data collected at Col de Porte. They found that CROCUS predicted daily snow temperatures reasonably well. Jordan (1991) compared transfer coefficients modelled by SNTHERM with snow temperature data as well as literature values and found them to be feasible. Cline (1997) showed that the SNTHERM-simulated latent heat flux over a snow season at a Colorado alpine site was similar to that determined with the aerodynamic profile method.

Results with discussion

Meteorological and surface conditions

This study covers 31 days from just prior to snowmelt to the end of the snow season. Initial mean snow depth for the plot was 640 mm with a SWE of 378 mm. There was 19 mm precipitation over the period; some light snowfall in early June and several rain showers from mid- to late June. Snow depth dropped in late May, but runoff did not appear until 8 June, snow-free patches were evident several days later and melt was complete on 24 June.

Summary statistics for the snowmelt period are given in Table 2. Regression analysis between the 10 min data sets (5328 data pairs) showed that the 2 and 10 m levels track each other extremely well with coefficients of determination of 0.95, 0.98 and 0.98 for relative humidity, wind speed and air temperature, respectively. This tendency is important as the APM is based on the similarity hypothesis which states that the latent heat flux is constant throughout the boundary layer.

Wind speed has the greatest variance: its fluctuation is related to the changing wind direction, with the strongest winds originating from the NW (Figure 2). There are two periods of several days in early and late June that recorded sustained high wind speeds from the north-west ($>6\,m\,s^{-1}$). Winds from the NW, SSW to SW and SSE register the greatest differences between the meteorological conditions observed by the two tower levels.

Air temperature had little variation (0–5°C) and rose steadily over the period: no negative values are recorded after 5 June (Figure 3). The daily range was around 3°C in late May and dropped to less than 2°C by the solstice. Between 2–6 June, the diurnal cycle of temperature was disrupted by high speed winds; the temperature dropped and then rose steadily. There are a few periods with temperature inversions, notably between 19–21 May and 7–11 June. When they occur, inversion temperature differences are typically less than 1°C.

Specific humidity fluctuates little before melt but rose sharply in early June (Figure 4). Prior to 5 June the average at the 2 m level is $3\,g\,kg^{-1}$, after this date humidity rose to $4.1\,g\,kg^{-1}$. Air with the lowest humidity is brought by north-westerly and southerly winds while the greatest humidity air flows from the north and east from Kongsfjord and the ocean. The humidity sensor has an accuracy of 3%: at low temperatures such an error can mean the difference between evaporation and condensation being simulated.

Modelled and measured latent heat flux

The latent heat fluxes modelled with the BPM within SNTHERM and CROCUS are very similar (Figure 5). The APM simulations track the BPM results until early June when melt starts. The trend follows SNTHERM and CROCUS for some days (values are $20–50\,W\,m^{-2}$ less), but, by the end of the melt season, the snow models simulate a small amount of condensation while the APM suggests evaporation rates of $3–4\,mm\,d^{-1}$ (around $100\,W\,m^{-2}$) with only a few hours of condensation estimated between 8–18 June. The divergence could be due to errors in humidity measurement, but it is more likely that the APM, which makes use of data collected at a height of 10 m, is responding to the development of bare soil patches. Divergence is particularly noticeable after 13 June when snow-free patches of several metres width were well developed, while by 18 June the bare soil covered over 50% of the ground surface. Other differences between the APM and snow models is the stability function calculation (for instance, the bulk Richardson number versus the profile Richardson number) and the use of default roughness length and bulk transfer coefficients in the snow models. Cline (1997) suggested this possibility when comparing the APM method with SNTHERM. He generally found good agreement; the greatest differences were associated with synoptic scale warm air advection. However, in Colorado, SNTHERM tended to predict greater flux values and variation rather than less as demonstrated here.

Table 2 Summary statistics for the variables measured at the meteorological tower

	2 m level			10 m level		
Variable	**Mean**	**Std dev**	**Range**	**Mean**	**Std dev**	**Range**
Wind speed ($m\,s^{-1}$)	2.5	2.0	0.7–10.2	2.9	2.5	0.7–10.6
Air temperature (°C)	1.1	2.4	−5.1–10.1	0.9	2.4	−5.6–9.8
Specific humidity ($g\,kg^{-1}$)	3.53	0.68	1.8–5.83	3.18	0.62	1.79–4.91

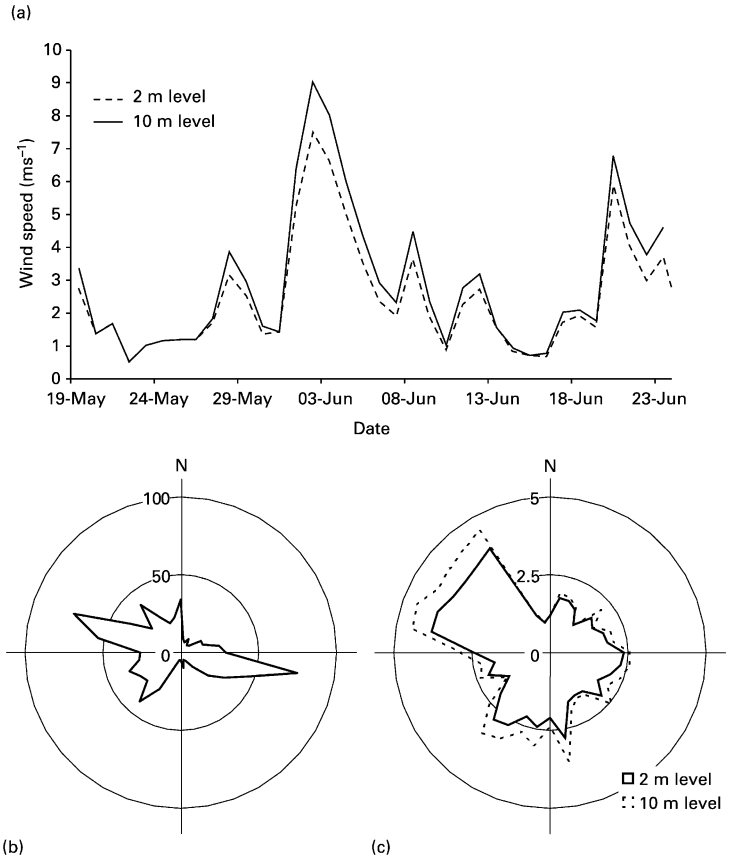

Figure 2 Wind characteristics. (a) Average daily wind speed, (b) wind direction hourly frequency, (c) hourly wind speed ($m\,s^{-1}$) as a function of wind direction. Roses are prepared using hourly data (895 points) and have plotting intervals of 10°

The APM predicts total latent heat losses from the snowpack for the 31-day investigation of 83.8 $MJ\,m^{-2}$ (equivalent to 33 mm evaporation); condensation is estimated to be around 1.8 $MJ\,m^{-1}$. Over the 10 days between melt initiation and large patch development (8–18 June) the latent heat flux was 16.9 $MJ\,m^{-2}$ – or 2% of the SWE lost to evaporation. The latent heat flux represents around 20–30% of the accumulated net radiation flux available at

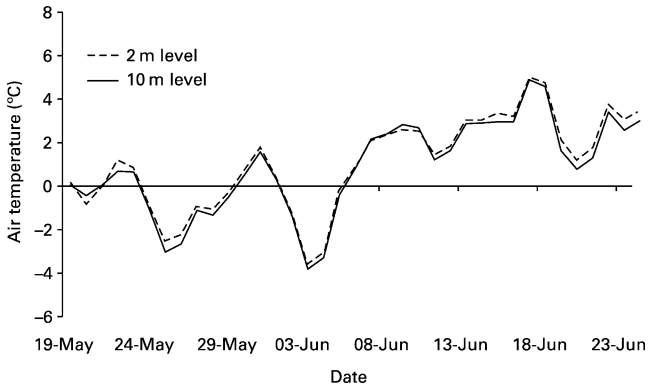

Figure 3 Average daily air temperature

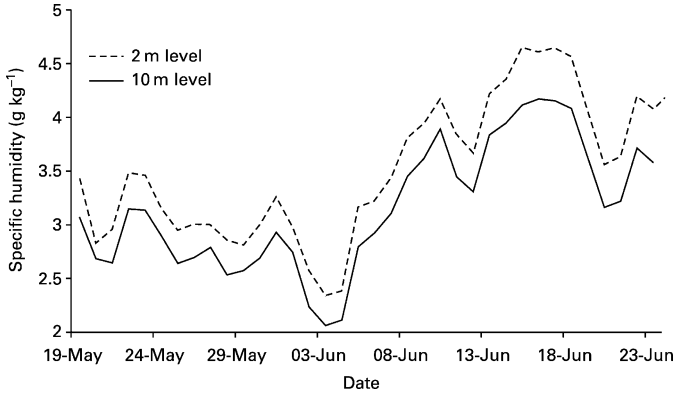

Figure 4 Average daily specific humidity

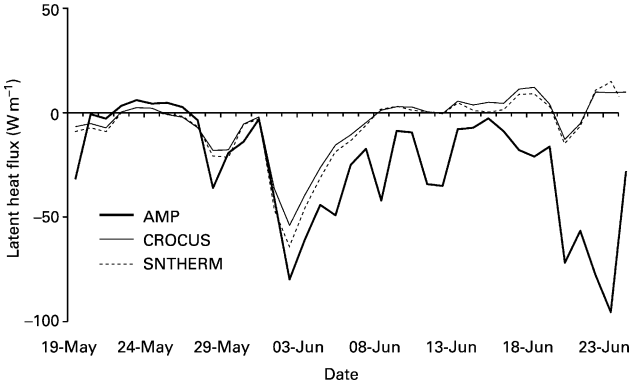

Figure 5 Latent heat flux modelled with the bulk and aerodynamic profile methods

the snow surface (Figure 6), which is similar to the proportion found when eddy correlation equipment was available (LAPP 1999; Harding and Lloyd 1998). Up until 27 May the APM estimates show a weak diurnal cycle not present in the snow model estimates; that is, a more strongly negative daytime flux.

SNTHERM and CROCUS each estimate approximately 26 MJ m^{-2} for evaporation and 5 MJ m^{-2} for condensation over the entire 31-day period. The net loss to the snowpack is around 2% of the SWE – that is, the evaporation predicted during early melt is mitigated by

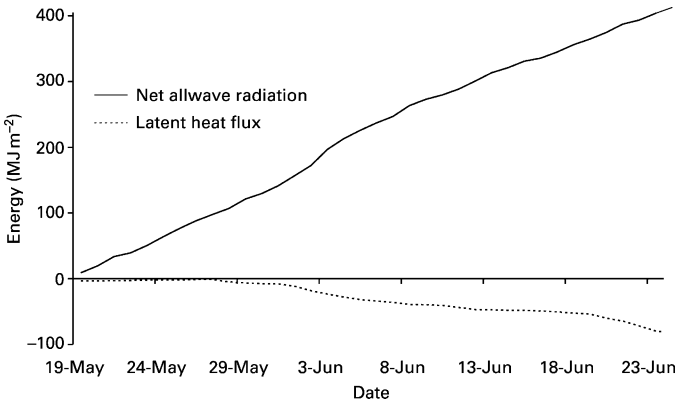

Figure 6 Cumulative net radiation and APM estimated latent heat fluxes over the investigation period

later condensation. Maréchal *et al.* (2002) found that both models tended to slightly underestimate snow surface temperature, particularly before runoff is recorded. Up until 5 June, when air temperature became positive, both models predict snow surface temperatures 2 or 3°C less than the almost constant 0°C measured. It is not until 9 June that the models predict an isothermal snowpack. A cold (dry) simulated snow surface means that losses to the snowpack predicted by the BPM are likely to be slightly less as the surface can no longer be assumed to be moist, i.e. sublimation vs evaporation.

Unfortunately, the period of direct measurements of evaporation and condensation from the six plastic containers is short. All three latent heat estimates just prior to and during early melt show a strongly negative flux from the snowpack. While the containers show the same general trend (evaporation), there are differences of up to 2 mm SWE between them. The set of containers closest to the IHL plot and tower is considered to be more representative of the modelled conditions and the average change in SWE is shown in Figure 7 with the simulated values. The total evaporation was 11 mm compared to 15, 9 and 7 mm for the APM, SNTHERM and CROCUS, respectively. Evaporation simulated by the APM, which gave the greatest rates, was less than 5% of the total SWE. Measured and modelled values of condensation were comparatively minor (< 1 mm).

Water balance calculations

One of the reasons for this study was the realisation that the runoff plots could not give reliable estimates of snowpack evaporation or condensation. An advantage of the BPM over the APM is that the method is embedded within snowmelt simulations which allows a comparison of simulated runoff with measured values. Runoff for the 1999 snowmelt season began to be recorded on 7 June. Both snowmelt models predicted runoff only a matter of hours later, but they also simulated melt for two days longer than actually occurred. Simulated snow depth tracked measured depth reasonably well. The measured runoff is greater than either model predicts (SNTHERM 386 mm; CROCUS 396 mm) and exceeds the sum of the observed SWE and precipitation (397 mm) for the investigation period. While it is possible that SWE was underestimated, it is more likely that the excess water flowed in from outside the plot area, either through the soil or over an ice layer lying above the soil (see Bruland and Maréchal 1999). Indeed, high discharge at the site continued for several days after the snow disappeared; the total discharge that can be associated with melt is 411 mm

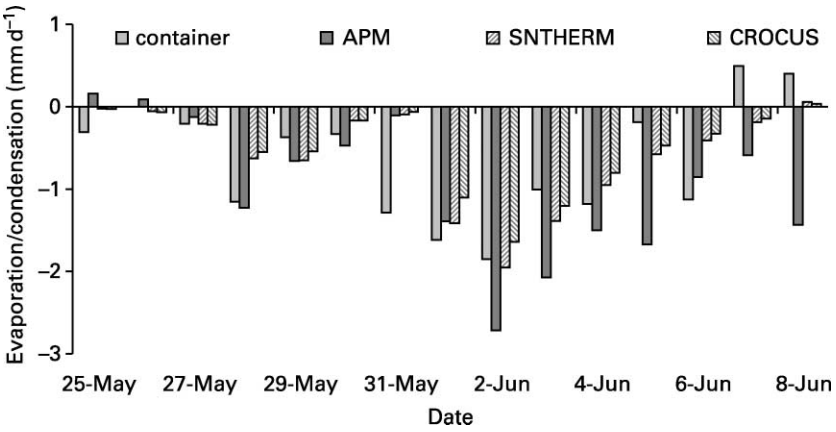

Figure 7 Measured and modelled daily snow evaporation (negative) and condensation (positive) near the IH lower runoff plot

before rain fell on 27 June. Hence, it was neither possible to estimate evaporation from the water balance nor to use the water balance to assess model performance.

Influence of wind direction

Simulated latent heat exchanges were investigated with respect to wind direction and other meteorological variables to identify the factors leading to evaporation and condendsation. Synoptic wind patterns at Leirhaugen are modified by the local topography. Figure 2 indicates a relationship between wind speed and wind direction; there are also similar links between wind direction and air temperature and relative humidity (Hanssen-Bauer *et al.* 1990). Hence, it can be expected that the latent heat flux exhibits a similar relationship to wind direction. A comparison of wind direction and latent heat modelled with each method (see Figure 8 for the APM example) shows a strong directional bias and resembles the wind frequency increase (Figure 2b). As the three methods of determining the heat flux gave the same basic pattern prior to patch formation, the discussion is limited to the APM.

ESE is the prevailing wind direction and 19% of the total evaporation occurs when the wind is from this direction. The air is cool and moist, so the rate of evaporation is moderate ($0.037\,\mathrm{mm\,h^{-1}}$). Winds from the glaciers to the SSE are associated with the highest evaporation rate ($0.048\,\mathrm{mm\,h^{-1}}$). However, these winds are not common and have little influence on seasonal evaporation (3%).

SSW and SW winds also come over mountains and ice and have similar wind speeds, temperature and humidity. Sixteen per cent of the seasonal evaporation occurs during periods with these wind directions and the evaporation rate is $0.06\,\mathrm{mm\,h^{-1}}$. Førland *et al.* (1997) showed that these winds are subject to orographic rise, with summer precipitation some 80% less at Ny-Ålesund than at gauges south of the mountains.

Winds from the WNW to NW are common. They flow from the open ocean over a mountain ridge; the velocity is fairly high and the air cool and dry. Twenty-nine per cent of the seasonal evaporation occurs when the wind is north-westerly and the average evaporation rate is $0.06\,\mathrm{mm\,h^{-1}}$. The dip in latent heat between 1–5 June occurred when there were NW winds with high velocities and very low air humidity. This period was covered by the container measurements and accounted for 24% of the total simulated evaporation. Another, period of NW winds occurred between 19–21 June and is captured by the three computation methods.

Condensation also shows a wind direction bias and is associated with winds from the N to E. These winds blow from Kongsfjord and seldom occur; they have low wind speed, moderate to high humidity and mild air temperatures.

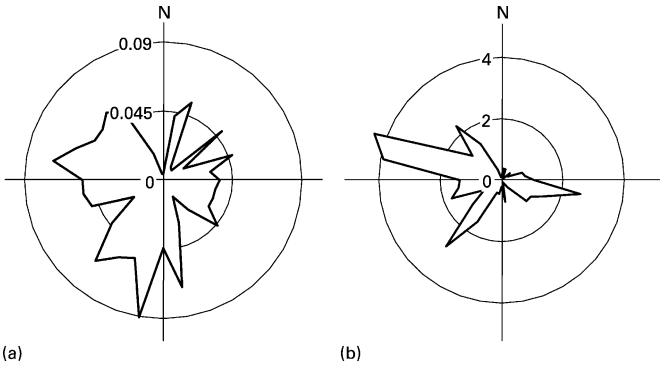

Figure 8 Dependence of APM estimated latent heat flux on wind direction. (a) Average rate of evaporation ($\mathrm{mm\,h^{-1}}$), (b) total evaporation (mm). Roses are prepared using hourly data (895 points) and have plotting intervals of 10°

Influence of microclimates

The difference between the BPM and APM simulations of latent heat are explained above by the height of the top level of the meteorological tower. That is, the latter method is influenced by an amalgam of snow covered and bare soil surface conditions while the former assumes a continuous snow cover. Meteorological conditions over a snowpack are subject to local variations in topography and land cover. A number of studies have shown that uneven pre-melt snow distribution drives the development snow-free patches (e.g. Shook and Gray 1996; Woo 1998; Luce *et al.* 1999). Snow-free patches are of great importance for small scale processes as they alter the near-surface wind, air temperature and humidity. When snow cover is continuous, vertical turbulent exchanges over the smooth surface are influenced by the regional air-mass characteristics and conditions reach a steady state. Once melt begins the surface becomes a mosaic of snow-covered and snow-free patches and the steady state breaks down. Bare soil has a lower albedo than snow (around 0.2 compared to 0.8) and can have a roughness length an order of magnitude greater. Variation of air temperature and stability over the two surface types causes complex airflow patterns of increased turbulence and localised warming so that snow receives heat locally advected from the bare patches (Marsh and Pomeroy 1996). Sensible heat advection is better documented than the latent heat flux and is therefore discussed in greater detail below: however, the heat exchange processes are similar.

Shook (1995) reports that measuring the sensible heat flux over melting prairie snow is fraught with difficulties due to changing wind direction and fetch over the uneven distribution of snow-covered and snow-free areas. As warm air from a snow-free patch moves across snow, a boundary layer forms downwind of the snow leading edge, causing the development of large vertical and horizontal gradients in the variables that drive the turbulent fluxes. Where the air temperature is greater than 0°C, the sensible heat flux must be downwards to the snow surface. Advection decreases exponentially with distance from the snow leading edge (Weisman 1977). Liston (1995) developed a numerical atmospheric boundary layer model to simulate local exchanges of momentum, heat and moisture for patchy snow. Model runs over a horizontal distance of 10 km simulated a range of snow-free patch sizes and snow cover percentages under constant meteorological conditions. With 50% snow-covered area and a snow-free fetch of 4 km followed by a 4 km stretch of snow, the latent heat is estimated to be around $-30\,\mathrm{W\,m^{-2}}$ at the snow leading edge whereas 1 km distant it is slightly positive. Sensible heat also increased. The total energy available to snowmelt rose by up to 30% as larger areas upwind of the snow became exposed.

Marsh *et al.* (1997) show that the relationship between atmospheric temperatures at the 850 mb level diverges sharply from the near-surface air temperature as snowmelt progresses due to solar warming of snow-free patches which in turn warms the overlying air. Neumann and Marsh (1998) used three temporary meteorological stations over snow separated by 400 m to measure sensible heat advection from a snow-free surface. They largely confirmed the pattern found by Liston (1995). Marsh *et al.* (1999) used a boundary layer modelling routine with variable climate and patch data including patch size and total snow coverage. The model estimated that sensible heat can be more than 750% greater at the leading edge of a 4 km long snow cover than at 1 km distant.

At the Leirhaugen site, Bruland *et al.* (2001b) found that snow accumulation patterns are dependent on local topography and wind patterns, leading to patch development upon melt. Even though the snow and bare soil patches were not as large as those modelled by Liston (1995) and Marsh *et al.* (1999), it is reasonable to expect local advection. The albedo of bare soil recorded just after melt in June 1999 was between 0.08–0.11 compared to 0.42–0.58 for adjacent snow. Lloyd *et al.* (2001) found that the surface albedo at Leirhaugen dropped from 0.7 to less than 0.1 within days of the commencement of snowmelt during 1995 due to the

exposure of bare soil. They also recorded that the soil surface warmed rapidly to between 1 and 4°C (cf snow 0°C). The surface roughness length is up to 1 cm for the soil compared to 1.5 mm for snow; Lloyd *et al.* (2001) found a median roughness length of 3 mm over the largely bare soil surface. The effect of snow-free patches can also be seen in the eddy correlation measurements for the 1995 and 1996 snow seasons (Lloyd 2000 personal communication). It was found that the sensible heat flux tended to be negative after 10 June in 1995 and 16 June in 1996 when the snowpack was sufficiently shallow to allow bare soil to appear and an active layer to develop. Advection of sensible heat from the soil to the atmosphere represents a possible energy gain for neighbouring snow.

Local advection affects both the bulk and aerodynamic profile methods of determining the turbulent heat fluxes. Each has fundamentally different lower boundary conditions. The former calculates the fluxes between meteorological conditions at a single level (2 m) and the snow surface which is constrained by a maximum temperature of 0°C and is at or near saturation humidity. The APM in contrast calculates between meteorological conditions at two heights (2 and 10 m) and has no lower boundary restrictions. SNTHERM and CROCUS predict condensation onto the snow surface during late melt largely in response to warm moist air entrained over the developing soil active layer. This surface temperature inversion is not evident between the two tower data sets which represent the average situation. The APM method gives the average latent heat flux over snow-free and snow-covered patches whereas the bulk profile method is applicable only to the snow surface. If the upper level of the tower had been lower, it could be expected that the APM would give estimates more in keeping with the BPM estimates.

Conclusions

This study is part of a series which seek to determine and model land surface/atmospheric interactions at a joint UK/Norwegian administered Arctic research station near Ny-Ålesund, Spitsbergen, Svalbard Archipelago. The objectives were to assess models for calculating latent heat fluxes over a melting snowpack and to determine the land and atmospheric conditions which drive evaporation at the site. The bulk and aerodynamic profile methods of computing latent heat fluxes over a snowpack were compared for the 1999 melt season. The BPM is embedded in the physically based SNTHERM and CROCUS snowmelt models. As this method hinges on the momentum and vapour gradients between the snow surface and near-surface climate observations, each model must keep a running tally of incoming and outgoing energy and mass fluxes to determine the snowpack surface roughness, temperature and humidity. The APM is fundamentally different in that it calculates the gradients between climatic observations made at two different heights and does not require snow-surface data as input.

The three sets of latent heat flux estimates were similar prior to and during the main melt period, but the APM tended to give much larger negative estimates. Comparison against average evaporation measured for two weeks as the daily weight difference from six snow-filled containers suggests that the APM overestimates evaporation while the snow models underestimate. However, the differences between the methods are no greater than those observed between individual containers. While a minor part of the water balance ($>5\%$ of the total SWE), the APM estimated latent heat flux represents 30% of the net all-wave radiation during the melt period before patches of bare soil appeared. This value is comparable to the proportion determined during earlier snow seasons using eddy correlation. All three models estimate less evaporation than determined by other Arctic studies which suggest upwards of 10% SWE can be lost to evaporation or sublimation. There is a clear relationship between wind direction and the latent heat flux. Around 30% of the evaporation calculated with the APM and over half

that calculated by either snow model occurred during periods with high velocity north-westerly winds.

All three sets of estimates show that some condensation occurs. The two snow models predict condensation almost exclusively during the final days of melt while the APM shows strongly negative latent heat exchanges. The difference in results between the methods suggests that there are energy and mass transfers from snow-free patches. Both the bulk method and APM are affected by local heat advection: however, as the latter is influenced by snow-covered and snow-free surfaces (higher albedo and roughness) by virtue to the tower height, it predicts average or effective evaporation. In contrast, the bulk profile method applies strictly to the snow surface. The maximum surface temperature of 0°C leads to permanent temperature inversion being registered during much of the late melt season, resulting in condensation. It seems that none of the models is able to capture real-world complexities related to the development of a patchy snow cover with the data available.

Acknowledgements

Annette Semadeni-Davies would like to thank NorFA and the Hellmuth Hertz Foundation for jointly funding her post-doctoral scholarship at the Norwegian University of Science and Technology. Yuji Kodama received funding from Overseas Research Aid, Japanese Ministry of Education, Science, Sports and Culture.

References

Anderson, E.A. (1976). A point energy and mass balance model of a snow cover. *NOAA Tech. Rep.*, NWS 19.

Andreas, E.L. and Murphy, B. (1986). Bulk transfer coefficients for heat and momentum over leads and polynyas. *J. Phys. Oceanogr.*, **16**(11), 1875–1883.

Bengtsson, L. (1980). Evaporation from a snow cover. *Nordic Hydrol.*, **11**, 221–234.

Bruland, O. and Maréchal, D. (1999). *Energy- and Water Balance of the Active Layer, 1991–1994. Understanding Land Arctic Physical Processes 1996–1998*. Technical Report STF22A98417. SINTEF Civil and Environmental Engineering, Trondheim, Norway.

Bruland, O., Maréchal, D., Sand, K. and Killingtveit, Å. (2001a). Energy and water balance studies of a snow cover during snowmelt period at a high arctic site. *Theor. Appl. Climatol.*, **70**(1–4), 55–63.

Bruland, O., Sand, K. and Killingtveit, Å. (2001b). Snow distribution at a high arctic site at Svalbard. *Nordic Hydrol.*, **32**(1), 1–12.

Brun, E., David, P., Sudul, M. and Bruno, G. (1992). A numerical model to simulate snow-cover stratigraphy for operational avalanche forecasting. *J. Glaciol.*, **38**, 13–22.

Brun, E., Martin, E., Simon, V., Gendre, C. and Coléou, C. (1989). An energy and mass model of snow cover suitable for operational avalanche forecasting. *J. Glaciol.*, **35**, 333–342.

Burns, R. (1785). *To A Mouse, On Turning Her Up In Her Nest With The Plough*.

Businger, J.A. (1973). Turbulent transfer in the atmospheric surface layer. In D.A. Haugen (Ed.), *Workshop on Micrometeorology*. American Meteorological Society, Boston, MA, pp. 67–100.

Cline, D.W. (1997). Snow surface energy exchanges and snowmelt at a continental, multitude Alpine site. *Wat. Res. Res.*, **33**(4), 689–701.

Deardorff, J.W. (1968). Dependence of air-sea transfer coefficients on bulk stability. *J. Geophys. Res.*, **73**(8), 2549–2557.

Essery, R., Martin, E., Douville, H., Fernandez, A. and Brun, E. (1999). A comparison of four snow models using observations from an alpine site. *Climate Dyn.*, **15**, 583–593.

Førland, E.J., Hanssen-Bauer, I. and Nordli, P.Ø. (1997). *Orographic Precipitation at the Glacier Austre Brøggerbreen, Svalbard*. DNMI klima report no. 02/97. The Norwegian Meteorological Institute, Oslo.

Hanssen-Bauer, I., Kristensen Solås, M. and Steffensen, E.L. (1990). *The Climate of Spitsbergen*. DNMI report no. 39/90. The Norwegian Meteorological Institute, Oslo.

Harding, R.J. and Lloyd, C.R. (1998). Fluxes of energy and water from three high latitude tundra sites in Svalbard during the snowmelt and snowfree periods. *Nordic Hydrol.*, **29**(4/5), 267–284.

Jordan, R. (1991). *A One-dimensional Temperature Model for a Snow Cover: Technical Documentation for SNTHERM89*. Special Report 91–16. US Army Cold Regions Research and Engineering Laboratory, Hanover, NH.

Kane, D.L., Hinzman, L.D., Benson, C.S. and Liston, G.E. (1991). Snow hydrology of a headwater Arctic basin 1. physical measurements and process studies. *Wat. Res. Res.*, **27**(6), 1099–1109.

LAPP (1999). *LAPP: Land Arctic Physical Processes*. Final report. Available online: http://www.nwl.ac.uk/ih/www/research/blapp.html. CEH Wallingford, UK.

Liestøl, O. (1977). Pingos, springs and permafrost in Spitsbergen. *Norsk Polarinstitutts Årsbok*, **1975**, 7–29.

Liston, G.E. (1995). Local advection of momentum, heat, and moisture during the melt of patchy snow covers. *J. Appl. Meteorol.*, **17**, 833–842.

Liston, G.E. and Sturm, M. (2003). The role of winter sublimation in the Arctic moisture budget. *Proc. 14th Northern Research Basins Symposium*, Greenland, August 25–29 2003, 91–98.

Lloyd, C.R., Harding, R.J., Friborg, T. and Aurela, M. (2001). Surface fluxes of heat and water vapour from sites in the European Arctic. *Theor. Appl. Climatol.*, **70**, 19–33.

Luce, C.H., Tarboton, D.G. and Cooley, K.R. (1999). Sub-grid parameterization of snow distribution for an energy and mass balance snow cover model. *Hydrol. Process.*, **13**, 1921–1933.

Male, D.H. and Granger, R.J. (1981). Snow surface energy exchange. *Wat. Res. Res.*, **17**(3), 609–627.

Maréchal, D., Sand, K. and Bruland, O. (2002). Comparison of two energy and mass balance models of snow cover for a high arctic site. (unpublished manuscript).

Marsh, P. and Pomeroy, J.W. (1996). Meltwater fluxes at an Arctic forest-tundra site. *Hydrol. Process.*, **10**, 1383–1400.

Marsh, P., Pomeroy, J.W. and Neumann, N. (1997). Sensible heat flux and local advection over a heterogeneous landscape at an Arctic tundra site during snowmelt. *Annals Glaciol.*, **25**, 132–136.

Marsh, P., Neumann, N.N., Essery, R.L.H. and Pomeroy, J.W. (1999). Model estimates of local advection of sensible heat over a patchy snow cover. In: *Interactions Between The Cryosphere, Climate and Greenhouse Gases. Proc. IUGG 99 Symp. HS2, Birmingham, July*, IAHS Publ. no 256. Wallingford, UK. 103–110.

Moore, R.D. and Owen, I.F. (1984). Controls on advective snowmelt in a maritime alpine basin. *J. Climate Appl. Meteorol.*, **23**, 135–142.

Neumann, N. and Marsh, P. (1998). Local advection of sensible heat in the snowmelt landscape of Arctic tundra. *Hydrol. Process.*, **12**, 1547–1560.

Ohmura, A. (1981). Climate and energy balance on Arctic tundra. Axel Heiberg Island, Canadian Arctic Archipelago, spring and summer, 1969, 1970, and 1972. *Zurcher Geographische Schriften*, **3**.

Ohmura, A. (1982). Evaporation from the surface of the Arctic tundra on Axel Heiberg Island. *Wat. Res. Res.*, **18**, 91–300.

Rydén, B.E. (1977). Hydrology of Truelove Lowland. In L.C. Bliss (Ed.), *Truelove Lowland, Devon Island, Canada: A High Arctic Ecosystem*, University of Alberta Press, Edmonton, pp. 107–136.

Saucier, W.J. (1983). *Principles of Meteorological Analysis*, Dover, New York.

Shook, K. (1995). Simulation of the ablation of prairie snowcovers. *PhD thesis* University of Saskatchewan, Saskatoon.

Shook, K. and Gray, D.M. (1996). Small-scale spatial structure of shallow snowcovers. *Hydrol. Process.*, **10**, 1283–1292.

Weisman, R. (1977). Snowmelt: a two-dimensional turbulent diffusion model. *Wat. Res. Res.*, **13**(2), 337–342.

Woo, M.-K. (1998). Arctic snow cover information for hydrological investigations at various scales. *Nordic Hydrol.*, **29**(4/5), 245–266.

Woo, M.-K. and Young, K.L. (1997). Hydrology of a small drainage basin with Polar Oasis Environment, Fosheim Peninsula, Ellesmere Island, Canada. *Permafrost Periglacial Process.*, **8**, 257–277.